

SCIENTIFIC REPORTS



OPEN

Integration of inherent and induced chirality into subphthalocyanine analogue

Luyang Zhao¹, Dongdong Qi¹, Kang Wang¹, Tianyu Wang¹, Bing Han², Zhiyong Tang² & Jianzhuang Jiang¹

Received: 05 April 2016

Accepted: 26 May 2016

Published: 13 June 2016

Conventional conjugated systems are characteristic of only either inherent or induced chirality because of synthetic challenge in combination of chiral segment into the main chromophore. In this work, chiral binaphthyl segment is directly fused into the central chromophore of a subphthalocyanine skeleton, resulting in a novel type of chiral subphthalocyanine analogue (*R/S*)-**1** of integrated inherent and induced chirality. Impressively, an obviously enhanced optical activity is discerned for (*R/S*)-**1** molecules, and corresponding enhancement mechanism is elucidated in detail. The synthesis strategy based on rational molecular design will open the door towards fabrication of chiral materials with giant optical activity, which will have great potential in chiroptical devices.

Chirality describes the geometric property of an object being non-superposable on its mirror image, which is omnipresent in nature^{1,2}. Due to the major role of the naturally occurring chlorophyll and vitamin B₁₂ in life science, chiral porphyrins and their artificial analogues, chiral phthalocyanines, have attracted extensive research interest in the past several decades^{3–5}. Study in this area has been significantly focused on exploration of varied molecular structures with strong optical activity in the UV-Vis region, owing to not only unlocking the mystery of life but also their potential application in chiroptical devices⁶. Similarly to other chiral conjugated systems with planar molecular structure⁷, the chirality of porphyrins or phthalocyanines is generally produced *via* two ways: (1) chiral arrangement of the achiral pyrrole/isoindole segments with the help of substituents, endowing the whole molecule with the inherent chirality^{8,9}; or (2) covalent attachment of additional chiral conjugated fragments onto the tetrapyrrole periphery, resulting in so-called induced chirality^{10,11}. Nevertheless, the lack of chiral segment in the central tetrapyrrole chromophore constitutes the primary and common feature of all the reported chiral porphyrins and phthalocyanines, regardless of their either inherent or induced chirality nature. As a result, only the relatively weak optical activity is discerned on these chiral tetrapyrrole derivatives, which in turn severely limits their potential applications in chiroptical field^{2,12}. Thus, it is highly desirable for creation of chiral conjugated systems with intrinsically structural difference from conventional analogues, development of theoretical models to guide design of chiral molecules with strong optical response, and achievement of giant optical activity from new chiral structures.

The ring-contracted homologue of phthalocyanine, subphthalocyanine, is known to possess a bowl-shaped geometrical structure, so it is expected to easily produce chirality compared with phthalocyanine due to absence of a symmetrical plane^{13–18}. As clearly demonstrated in Fig. 1(a), chiral arrangement of the central triisindole/tripyrrole with the help of peripheral substituents (symbol “X” in (a)-1, (a)-2 and (a)-3) makes these molecules generate inherent chiral asymmetry, C₃. Alternatively, incorporation of three chiral binaphthyl substituents onto the subphthalocyanine periphery affords the first but the sole example of subphthalocyanine with induced chirality (Fig. 1(b))¹⁵. Similarly to the ring-expanded tetrapyrrole homologues, all these subphthalocyanines with either inherent or induced chirality nature exhibit weak molecular dissymmetry as evaluated by the small value of their anisotropic factor *g*, $0.2 \times 10^{-3} \sim 0.6 \times 10^{-3}$ (Table 1)^{15,18,19}.

Herein, with subphthalocyanine chromophore as the basic conjugated building block, a new strategy is employed towards constructing chiral conjugated system. Direct fusion of the chiral segment, binaphthyl moiety, into the central chromophore of subphthalocyanine skeleton results in a pair of enantiopure isomers (*R/S*)-**1** with

¹Beijing Key Laboratory for Science and Application of Functional Molecular and Crystalline Materials, Department of Chemistry, University of Science and Technology Beijing, Beijing 100083, China. ²Laboratory of Nanomaterials, National Center for Nanoscience and Technology, Beijing 100190, China. Correspondence and requests for materials should be addressed to Z.T. (email: zytang@nanocr.cn) or J.J. (email: jianzhuang@ustb.edu.cn)

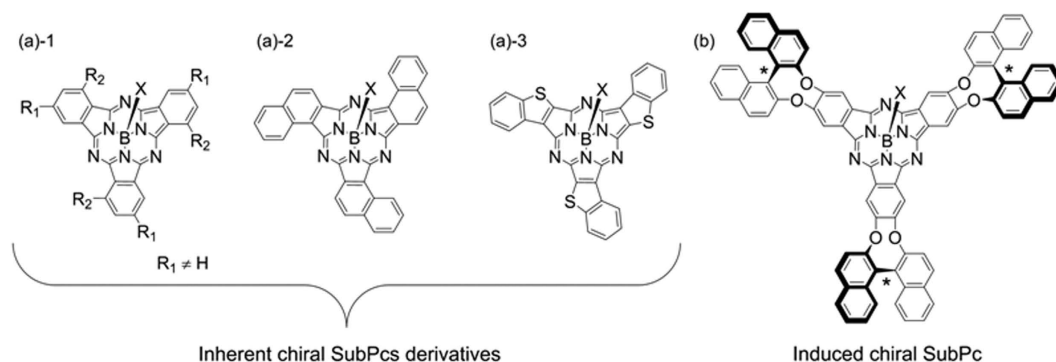


Figure 1. Molecular structures of conventional chiral subphthalocyanine derivatives with inherent (a) and induced chirality (b). Asterisk indicates locally chiral structure.

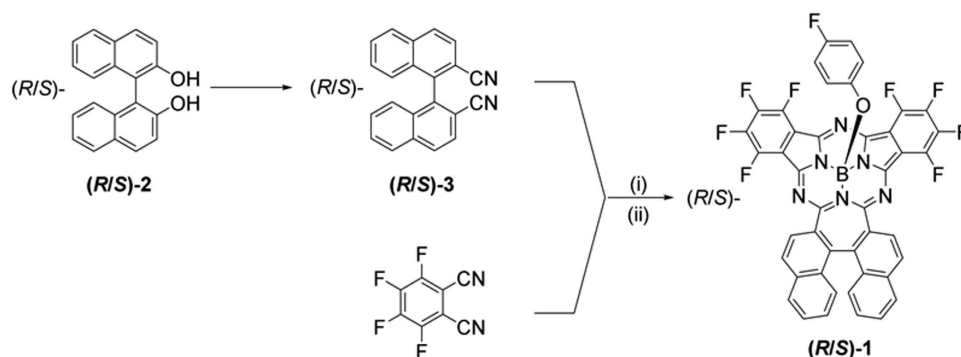


Figure 2. Synthesis of chiral subphthalocyanine analogue (*R/S*)-1. (i) BBr_3 , chlorobenzene, 60°C ; (ii) 4-Fluorophenol, 90°C .

Compound	Absorption band	Abs. ($10^4 \epsilon$)	Inherent CD ($10^3 \theta$)	Induced CD ($10^3 \theta$)	$10^{-3} g$
1	Q ₁	2.4	–	0.83	1.0
	Q ₂	3.6	–	1.05	0.88
	l-Soret	1.3	1.58	–	3.7
(b) ^[a]	Q	10.0	–	2.01	0.61
(a)-3 ^[a]	l-Soret	3.8	0.25	–	0.20

Table 1. Comparison of anisotropic factor, g , of **1** with that of two conventional chiral subphthalocyanine derivatives reported previously. [a] Shown in Fig. 1.

obviously enhanced optical activity (g values reach $0.88 \times 10^{-3} \sim 3.7 \times 10^{-3}$). It deserves stressing that significantly different from optical response of the conventional chiral subphthalocyanine derivatives, (*R/S*)-**1** displays both the inherent chirality characteristics in the Soret band region and the induced chirality in the Q-band range. This work represents the first chiral conjugated system with integrated inherent and induced chirality, which will open a new avenue towards fabrication of novel chiral conjugated systems with enhanced optical activity as well as shed light on possible application in the chiroptical devices.

Results and Discussion

Molecular design, synthesis, and characterization. Synthesis of the chiral intermediate, 1,1'-binaphthalene-2,2'-dicarbonitrile (**3**), is the key to directly integrate the chiral 1,1'-binaphthalene moiety into the central conjugated system of a subphthalocyanine analogue with help of the second species of achiral phthalonitrile²⁰. Starting from commercially available chiral binaphthol (*R/S*)-**2**, 1,1'-binaphthalene-2,2'-dicarbonitrile (*R/S*)-**3** was obtained in a total yield of 21% by seven steps (Scheme S1 in Supporting Information). Subsequent cyclo-trimerization of (*R/S*)-**3** and tetrafluorophthalonitrile in the presence of boron tribromide (BBr_3) in chlorobenzene at 60°C , followed by treatment with 4-fluorophenol at 90°C to displace the axial ligand, generated the target chiral subphthalocyanine analogue (*R/S*)-**1** in a yield of *ca.* 13%. As clearly demonstrated in Fig. 2, direct fusion

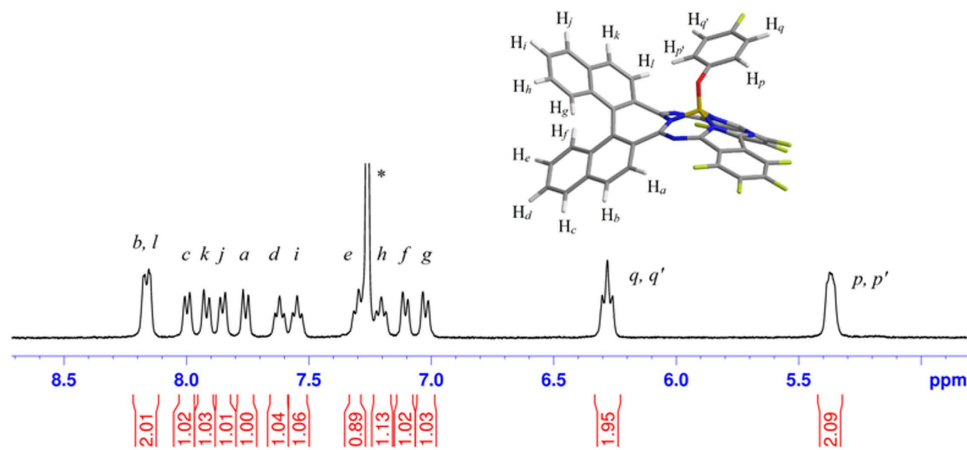


Figure 3. ^1H NMR spectrum with proton assignment of **1** recorded in CDCl_3 . The asterisk indicates the solvent impurity.

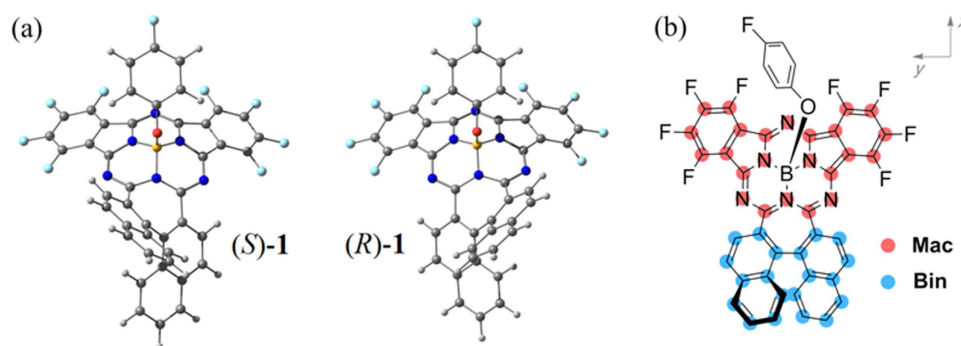


Figure 4. (a) Simulated molecular structures of (*S*)-**1** and (*R*)-**1** on basis of DFT calculations at M06/6-311G(d) level, and (b) scheme of molecular division into **Mac** and **Bin** groups.

of the chiral 1,1'-binaphthalene moiety into the central main conjugated chromophore of the subphthalocyanine analogue (*R/S*)-**1** renders this chiral compound intrinsically different structural feature from conventional chiral subphthalocyanine derivatives with either inherent or induced chirality (Fig. 1).

This new chiral subphthalocyanine analogue gives satisfactory elemental analysis data. Its matrix assisted laser desorption ionization time-of-flight (MALDI-TOF) mass spectrum displays intense signals for both a molecular ion signal $[\text{M}]^+$ and an axial-ligand-lost ion signal $[\text{M}-\text{OC}_6\text{H}_4\text{F}]^+$ with the isotopic pattern closely resembling the simulated one (Figure S1 in Supporting Information). To further clarify its molecular structure and optical property, this subphthalocyanine analogue was characterized with different spectroscopic techniques including nuclear magnetic resonance (NMR), electronic absorption (UV-Vis absorption), circular dichroism (CD), and magnetic CD (MCD) spectroscopy.

Figure 3 shows the ^1H NMR spectrum of **1** recorded in CDCl_3 at room temperature. Evidently, each of the binaphthyl protons exhibits a discrete signal due to the C_1 molecular symmetry. With the help of ^1H - ^1H COSY and NOESY measurements, all the protons are assigned in an unambiguous manner (Figures S2 and S3, and Table S1 in Supporting Information). The signals with chemical shift at $\delta = 8.16, 8.00, 7.76, 7.62, 7.31$ and 7.11 ppm are attributed to a set of six protons on the inner side (*endo*) of the naphthene moiety bearing a higher deshielding effect, while the ones at $\delta = 8.16, 7.92, 7.85, 7.55, 7.20$ and 7.02 ppm are assigned to the set of six protons on the outer side (*exo*) of naphthene moiety. It is worth noting that in the NOESY spectrum, two spatial couplings of H_b - H_c and H_j - H_k with distance of 2.43 \AA for both are clearly found, confirming the above-mentioned assignment of protons. One can also notice from Fig. 3 that owing to the different induced ring current, every *endo* proton shows a larger chemical shift than its corresponding *exo* proton except for H_l (*exo*, $\delta = 8.16$) and H_a (*endo*, $\delta = 7.76$). The small shift for H_l and H_a is likely to originate from the additional deshielding effect from the free-rotating axial 4-fluorophenoxy group.

Molecular structure. Trials paid so far failed to produce single crystals of (*R/S*)-**1** suitable for X-ray diffraction analysis. As a consequence, the molecular structure of enantiomers (*R/S*)-**1** pair with typical chiral asymmetry, C_1 , was simulated on the basis of density function theory (DFT) calculations at M06/6-311G(d) level, and the corresponding result is summarized in Fig. 4(a)²¹. As shown in the calculation result (Fig. 4(b)), the length of the two C-C bonds that connect the central core-modified chromophore **Mac** and binaphthyl unit **Bin** is 1.48 \AA , which locates just in the range of aromatic conjugated systems. This result manifests that these two moieties are

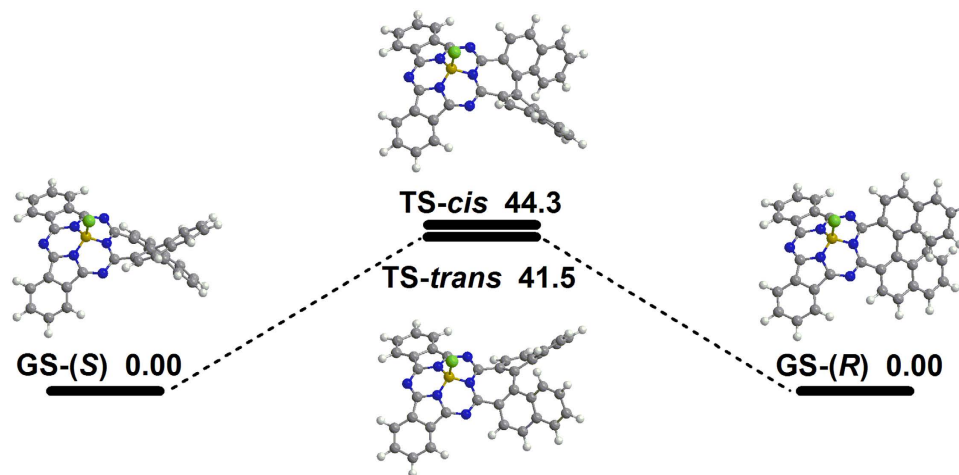


Figure 5. Configuration of ground states (GS) and transition states (TS) of **1** together with corresponding energy barrier ($\text{kcal} \cdot \text{mol}^{-1}$).

integrated into the conjugated system in **1**. Actually, anisotropy of the induced current density (AICD) analysis confirms again that the π -electron delocalization region is extended over the whole molecular skeleton of **1** (Figure S5 in Supporting Information)²². Obviously, direct fusion of the intrinsic chiral segment, the binaphthyl unit, into the conjugated molecular structure of **1** endows this chiral subphthalocyanine analogue intrinsically different structural feature from conventional chiral conjugated systems, which do not contain chiral segment in the central conjugated chromophore.

The chiral stability of this novel subphthalocyanine analogue is also uncovered by both DFT transition state calculations (Fig. 5) and chiral HPLC technique, Figure S7 (Supporting Information). DFT calculations for transition structures and internal reaction coordinate (IRC) paths (Figure S9, Supporting Information) show that the transition states of **1** exhibit *cis*- and *trans*-configurations with C_s molecular symmetry. The energy barriers of the two transition states resulting from the steric hindrance between two naphthene segment are up to 44.3 and 41.5 $\text{kcal} \cdot \text{mol}^{-1}$, respectively, which are difficult to be overcome below 200 °C. Such a large energy barrier guarantees enough thermo-stability for each enantiomer during the synthetic procedure. The enantiopurity of the final product (*R*)-**1** and (*S*)-**1** was confirmed by chiral HPLC (column: CHIRALPAK IA-3; eluent: propanol:hexane = 10:90) experiment result. As shown in the top of Figure S7 (Supporting Information), under the above-mentioned experimental condition the retention time for (*R*)-**1** and (*S*)-**1** amounts to 11.3 and 10.0 min, respectively. Nevertheless, no detectable enantiomeric fraction could be found for either (*R*)-**1** or (*S*)-**1**, middle and bottom of Figure S7 (Supporting Information).

Circular dichroism properties. The optical property of (*S*)-**1** and (*R*)-**1** is thoroughly characterized by the electronic absorption, CD and MCD spectra. In the electronic absorption spectrum, two absorption bands observed at 692 and 528 nm are attributed to the Q-bands (denoted as Q₁- and Q₂-band, respectively) of subphthalocyanine analogue with remarkable split resulting from the distorted molecular structure (bottom curve in Fig. 6)²⁰. In addition, **1** has a weak absorption at 435 nm in the low-energy Soret band region, followed by an intense absorption at 343 nm belonging to the high-energy Soret band^{18,23}. In the MCD spectrum (top curve in Fig. 6), a negative signal and a positive signal featured as two Faraday-*B* terms are observed at 690 and 529 nm in the Q-band region, indicating their homogeneous π - π^* transition nature with corresponding transitions localized on the main conjugated chromophore. The other two MCD peaks, a positive MCD signal at 443 nm in the low-energy Soret band region and a negative signal at 343 nm in the high-energy Soret band region, are also featured as Faraday-*B* terms. Finally, the optical activity of (*S*)-**1** and (*R*)-**1** pair is investigated by CD spectra (middle curves in Fig. 6). It is clear that the two isomers show perfect spectral mirror image over the entire region, confirming their enantiomeric molecular structures. In detail, along with the increased energy, (*S*)-**1** presents two negative CD signals at 698 and 530 nm in the Q-band region, a positive signal at 431 nm in the low-energy Soret band region, and again a negative signal at 348 nm in the high-energy Soret band region. In a similar way, the peaks at the same region with reverse signals are observed for (*R*)-**1**.

Significantly, (*S*)-(-)- or (*R*)-(+)-1,1'-binaphthyl substituent is able to induce negative and positive CD signals, respectively, throughout the entire absorption region of both phthalocyanine and subphthalocyanine compounds^{5,15,24}. It is known that the induced CD intensity is proportional to $v_N v / (v_N^2 - v^2)$, where v_N and v are the absorption frequencies of binaphthyl group and subphthalocyanine chromophore, respectively²⁵. In our case, (*S*)-**1** containing (*S*)-binaphthyl moiety yields two negative Q-band CD signals at 698 and 530 nm ($v = 0.43 \times 10^{15}$ and $0.56 \times 10^{15} \text{ s}^{-1}$, respectively) with homogeneous π - π^* electron transitions, while the frequency of binaphthyl group v_N that cannot be extracted from the absorption spectrum is estimated to be $0.93 \times 10^{15} \text{ s}^{-1}$ according to DFT calculation result (see the Methods section for details). As a result, the ratio of the CD intensity against $v_N v / (v_N^2 - v^2)$ for the Q₂-band is calculated to be ~ 0.8 of that obtained for the Q₁-band (Table S2 in Supporting Information). The quite close ratio value for these two Q-bands confirms that both Q-bands follow the mechanism of the induced optical activity from peripheral binaphthyl group^{24,26}. (*R*)-**1** with (*R*)-binaphthyl

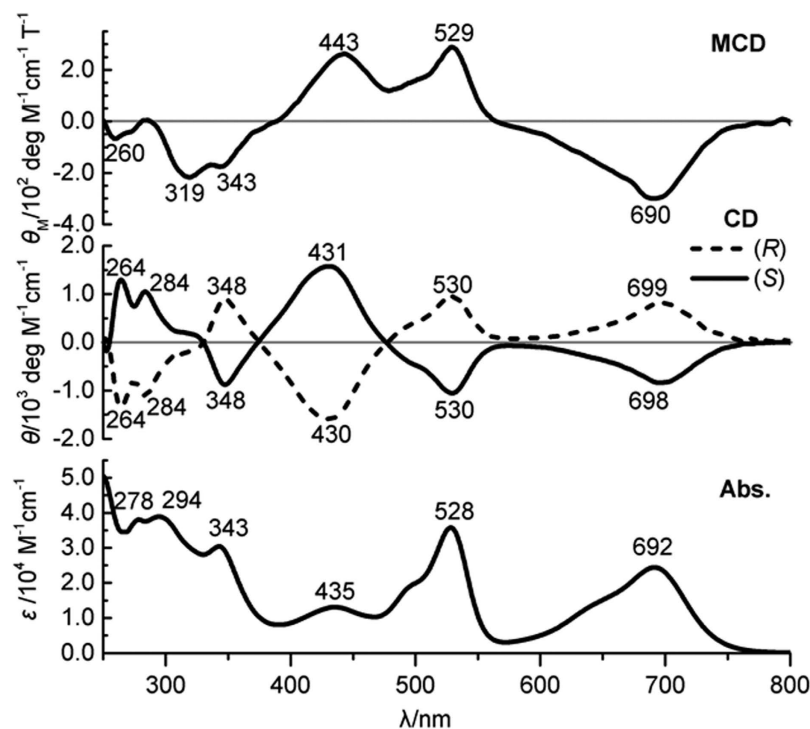


Figure 6. Electronic absorption, CD and MCD spectra of compound **1**.

moiety of two positive Q-band CD signals gives additional support for this point. As comparison, the ratio for the high-energy Soret band CD signal at 348 nm is only 0.07 of that obtained for the Q₁-band, denying the same chirality origin. This result clearly implies the inherent rather than induced chirality characteristics for the high-energy Soret band of **1**. Moreover, the CD signal of the low-energy Soret band at 431 nm is opposite with respect to the two Q-band CD responses, also disclosing the inherent chirality nature.

To quantitatively evaluate the chiral dissymmetry of this novel chiral subphthalocyanine analogue, the anisotropic factor g for **1** was calculated according to Equation (1)^{27,28}.

$$g = \frac{\Delta\varepsilon}{\varepsilon} = \frac{\varepsilon_L - \varepsilon_R}{\varepsilon_L + \varepsilon_R} = \frac{\theta}{33 \times \varepsilon} \quad (1)$$

where ε_L and ε_R are the molar extinction coefficients of left and right circularly polarized light, respectively, while θ and ε the ellipticity and absorbance that are directly obtained from the experimental spectra. Table 1 compares the g values of the subphthalocyanine analogue containing chiral segment in the central chromophore with those of conventional chiral subphthalocyanine derivatives with either inherent chirality ((a)-3 in Fig. 1) or induced chirality (b) in Fig. 1. It is evident that the g factor for the CD signals in the Soret bands of **1** is dramatically enhanced to 3.7×10^{-3} compared with *ca.* 2.0×10^{-4} of the reference compound (a)-3 in Fig. 1, thanks to the formation of a helical conjugated molecular structure with great chiral dissymmetry^{29–32}. On the other hand, the g factor for the CD signals of the Q-bands of **1** with induced chirality is also increased from *ca.* 6.1×10^{-4} of the reference compound (b) in Fig. 1 to 8.8×10^{-4} and 1.0×10^{-3} , largely because of the shortened distance, R_{ij} , between the chiral binaphthyl segment and the central conjugated chromophore of subphthalocyanine from *ca.* 9.2 Å for reference compound (b) (Fig. 1) to *ca.* 4.5 Å (measured from the simulated molecular structure in Fig. 4(a)). As demonstrated in the below Equation (3), the induced CD intensity is inversely proportional to the cube of the distance between the central conjugated chromophore and the chiral group, i.e., $\theta \propto R_{ij}^{-3}$, which is responsible for the increased g factor of the CD signal of the Q-bands of **1**. Considering such a fact that the Q-band CD signal of the reference compound is induced by three binaphthyl groups, while that of **1** by only one binaphthyl segment, the increase in the g factor from reference compound to **1** as detailed above clearly indicates the significant effect of the direct fusion of the binaphthyl segment into the central subphthalocyanine chromophore on the molecular dissymmetry of conjugated systems.

Electronic structure. On the basis of the quantum mechanics, the optical activity for chiral molecular compounds could be described by rotational strength, R :

$$R = \text{Im}(\boldsymbol{\mu} \cdot \boldsymbol{m}) \quad (2)$$

For the conjugated systems with inherent chirality, both $\boldsymbol{\mu}$ and \boldsymbol{m} are delocalized over the whole π system. In contrast, $\boldsymbol{\mu}$ and \boldsymbol{m} are decomposed to the contribution from either the main chromophore or additional chiral

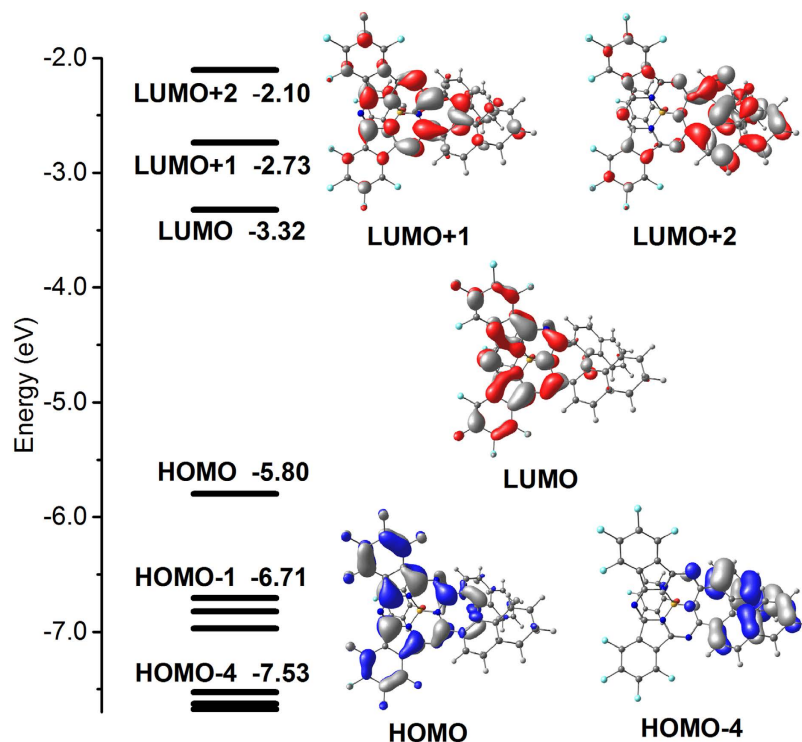


Figure 7. Diagram of frontier molecular orbitals of (S)-1.

substituent(s) for the conjugated systems with induced chirality, thus rendering an alternative way to calculate their rotational strength:

$$R = -\frac{2\nu_i V_{ij}}{h(\nu_j^2 - \nu_i^2)} \text{Im}(\boldsymbol{\mu}_i \cdot \mathbf{m}_j)$$

$$V_{ij} = \frac{1}{4\pi\epsilon_0} \left(\frac{\boldsymbol{\mu}_i \cdot \boldsymbol{\mu}_j}{|\mathbf{R}_{ij}|^3} - \frac{3\boldsymbol{\mu}_i \cdot \mathbf{R}_{ij} \boldsymbol{\mu}_j \cdot \mathbf{R}_{ij}}{|\mathbf{R}_{ij}|^5} \right) \quad (3)$$

in which subscripts i refers to the main conjugated chromophore with electric dipole-allowed transition moment $\boldsymbol{\mu}_i$ at energy $h\nu_i$, j represents the perturbation moieties [the additional chiral substituent(s)] in the molecule with electric dipole-allowed transition moment $\boldsymbol{\mu}_j$ and magnetic dipole-allowed transition moment \mathbf{m}_j (including both intrinsic and gauge-dependent external magnetic dipole moment) at energy $h\nu_j$, \mathbf{R}_{ij} stands for the distance between groups i and j , and V_{ij} is the Coloumb interaction coupling between the two moieties^{33,34}. As a result, a CD signal of the main conjugated chromophore with local electric dipole moment can be induced by coupling with the magnetic dipole moment of an external chiral group, leading to the original concept of induced optical activity. It should be pointed out that the existence of only Coulomb interaction between the main conjugated chromophore and additional chiral group(s) defines the essential feature of conjugated systems with induced chirality, while sufficient orbital correlation between neighboring components throughout the whole molecular skeleton determines the conjugated systems with inherent chirality nature.

Towards deep understanding of the spectral properties and chirality nature of this novel chiral subphthalocyanine analogue, DFT and time-dependent DFT (TDDFT) calculations have been performed at the M06/6-311G(d) level. Frontier molecular orbital (MO) patterns and their energy levels are illustrated in Fig. 7. Generally, HOMO, LUMO and LUMO + 1 mainly distribute on the subPc macrocycle, as highlighted in red in Fig. 4(b); while HOMO - 4 and LUMO + 2 mainly reside on the binaphthyl unit, as highlighted in blue in Fig. 4(b). Therefore, it is reasonable to divide the whole molecule into the main conjugated chromophore (**Mac**) segment and peripheral binaphthyl (**Bin**) segment. Figure 8 summarizes the TDDFT calculation results with the help of the electron density difference maps and fragment contributions. As can be seen, the Q₁-band absorption estimated at 647 nm is contributed almost exclusively by the transition HOMO → LUMO, which localizes mainly on the **Mac** moiety of 81.6 → 87.5% scale with only 18.4 → 12.5% electron exchange from **Bin**. Similarly, the Q₂-band absorption estimated at 502 nm is dominantly contributed by the transition HOMO → LUMO + 1 with the **Mac** moiety of 82.5 → 73.0%, suggesting a weak electron exchange from **Bin** with 17.5 → 27.0% in addition to the Coulomb interaction. The weak electron transition in the low-energy Soret band estimated at 413 nm is contributed by HOMO → LUMO + 2 with participation from the **Bin** part of 18.2 → 70.6%, indicating an intramolecular transfer from **Mac** to **Bin** with sufficient electron correlation between these two moieties. The high-energy Soret band

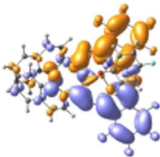
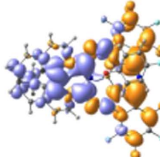
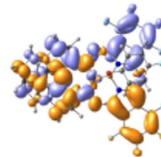
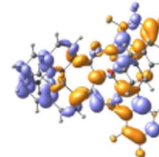
Band	Q ₁ -band	Q ₂ -band	Low-energy Soret band	High-energy Soret band
Electron transition density map ^[a]				
λ [nm]	647	502	413	349
f	0.16	0.43	0.17	0.12
R ^[b]	-85.5	-78.5	162.6	-86.9
Transition compositions ^[c]	H→L ^[d] 95%	H→L+1 95%	H→L+2 94%	H-4→L 39% H-5→L 42% H-6→L 5% H-7→L 6%
Electron exchange contribution from Bin ^[e]	18.4→12.5% ^[f]	17.5→27.0%	18.2→70.6%	56.2→11.9%
R_{Mac} (contribution) ^[g]	11.2 (-13.1%)	3.1 (-4.0%)	-	-

Figure 8. Calculated electronic transition density maps, excited wavelengths (λ), oscillator strengths (f), rotational strengths (R), and orbital compositions of important transitions of (*S*)-**1**. [a] The isovalue of electron transition density map is 0.008. [b] The unit is 10^{-40} erg-esu-cm/Gauss. [c] The transition compositions with more than 5% contribution are listed. [d] H refers to HOMO and L to LUMO. [e] Transition contribution of each fragment is summation of composed orbital contributions of each fragment. Orbital compositions more than 0.001% are counted. [f] From ground state to excited state. [g] Rotatory strength contribution is decomposed to **Mac** and **Bin** segments *via* Mulliken charge.

is composed by many weak transitions, among which the strongest transition contributed from inner occupied orbitals to LUMO calculated at 349 nm might correspond to the observed absorption at 343 nm^{18,35}. Interestingly enough, an intramolecular transfer from **Bin** to **Mac** with contribution from the **Bin** moiety of 56.2 → 11.8% is involved in this transition, also suggesting the sufficient electron exchange between these two moieties. Evidently, the two Q-band electron transitions are actually contributed dominantly by the **Mac** moiety with up to 84.6 and 77.8% on average, respectively, indicating the dominant Coulomb interaction between **Mac** and **Bin** and in turn disclosing the dominantly induced chirality characteristics for these two Q-band CD responses of **1**. This is in good agreement with the CD spectroscopic analysis as detailed above. However, this is not the case for both the low-energy Soret and high-energy Soret absorption bands. As indicated above, **Mac** moiety contributes 29.4% only to the excited state of the transition that is responsible for the low-energy Soret band, while the ground state of the transition responsible for the high-energy Soret band is contributed by 43.8% only from the **Mac** moiety, revealing the significant orbital correlation between **Mac** and **Bin** for these two Soret bands of **1**. This in turn confirms the inherent chirality characteristics of the two Soret-band transitions.

In addition, the induced chirality nature of the two Q-bands might be further revealed by CD contribution analysis with help of transition dipole moment decomposition, by which both the electric and magnetic transition dipole moments can be quantitatively decomposed into the contribution from group **Mac** and **Bin** (Fig. 4(b) and Table S3 in Supporting Information). The intrinsic rotational strength of **Mac** and **Bin** is obtained by direct scalar multiplication of their respective electric and magnetic transition dipole moments. As listed in Fig. 8, the rotational strength provided by **Mac** is calculated to amount to only -13.1% for the Q₁-band and -4.0% for the Q₂-band, respectively, with the rest totally originating from **Bin** as well as its interaction with **Mac**. Obviously, the **Mac** chromophore yields two Q-band CD signals largely caused by **Bin**. This confirms, again, the dominant induced chirality characteristics for the two Q-band CD signals. As comparison, the electron transitions that are responsible for both the low- and high-energy Soret bands spread over both **Mac** and **Bin** moieties, resulting in inapplicability of the transition dipole moment decomposition analysis for these two band transitions. Altogether, this novel subphthalocyanine analogue exhibits optical activity with both induced and inherent chirality nature, thus representing the first example of subphthalocyanine with mixed chirality characteristics.

Conclusion

In summary, chiral 1,1'-binaphthalene moiety has been directly fused into the conjugated skeleton of a subphthalocyanine analogue, resulting in an unprecedented chiral segment-containing π -conjugation system with improved chiral dissymmetry. Notably, this unconventional chiral subphthalocyanine analogue integrates inherent and induced chirality, which is significantly distinct from the conventional chiral subphthalocyanine derivatives only showing either inherent or induced chirality nature. As a result, this type of chiral subphthalocyanine analogue exhibits the significantly enhanced optical activity compared with conventional chiral

subphthalocyanines, and furthermore the origin of such improved optical activity is explored in detail by both experiment and theory. This work not only represents a brand new type of chiral conjugated system for device application, but also establishes the guideline towards rational design of chiral molecular structures with giant optical activity.

Methods

General remarks. Tetrahydrofuran (THF), triethylamine, chlorobenzene, and dichloromethane were freshly distilled from CaH_2 under nitrogen. Column chromatography was carried out on silica gel (Merck, Kieselgel 60, 70–230 mesh) columns with the indicated eluents. The electrolyte $[\text{Bu}_4\text{N}][\text{ClO}_4]$ was recrystallized twice from acetone. All other reagents and solvents were of commercial reagent grade and used as received. NMR spectra were recorded on a Bruker DPX 400 spectrometer in indicated solvent, using residual CHCl_3 solvent resonance as an internal reference for ^1H ($\delta = 7.26$ ppm) and $\text{BF}_3 \cdot \text{OEt}_2$ as an external reference for ^{11}B ($\delta = 0.00$ ppm). Elemental analyses were performed on an Elementar Vavio El III. HPLC was performed on a LC-9210NEXT instrument of JAI Co., Ltd. equipped with a preparative CHIRALPAK IA-3 column (250 mm) by monitoring absorbance at 528 nm. Electronic absorption spectra were recorded on a Hitachi U-4100 spectrophotometer. CD and MCD spectra were recorded on a JASCO J-1500 spectropolarimeter equipped with a JASCO electromagnet which produced both parallel and anti-parallel magnetic fields of 1.60 T. IR spectra were recorded in KBr pellets with 2 cm^{-1} resolution using a Bruker Tensor 37 spectrometer. MALDI-TOF mass spectra were taken on a Bruker BIFLEX III ultrahigh resolution Fourier transform ion cyclotron resonance (FT-ICR) mass spectrometer with alpha-cyano-4-hydroxycinnamic acid as matrix. Electrochemical measurements were carried out with a BAS CV-50W voltammetric analyzer. The cell comprised inlets for a glassy carbon disk working electrode of 2.0 mm in diameter and a silver-wire counter electrode. The reference electrode was Ag/Ag^+ , which was connected to the solution by a Luggin capillary whose tip was placed close to the working electrode. It was corrected for junction potentials by being referenced internally to the ferrocenium/ferrocene (Fc^+/Fc) couple [$E_{1/2}(\text{Fc}^+/\text{Fc}) = 501\text{ mV vs. SCE}$]. Typically, a 0.1 mol dm^{-3} solution of $[\text{Bu}_4\text{N}][\text{ClO}_4]$ in CH_2Cl_2 containing 0.5 mmol dm^{-3} of sample was purged with nitrogen for 10 min, then the voltammograms were recorded at ambient temperature. The scan rate was $75\text{ mV} \cdot \text{s}^{-1}$ for cyclic voltammetry measurement.

Preparation of (R/S)-1. To a chlorobenzene (0.5 mL) solution of **3** (76.0 mg, 0.25 mmol) in a 10 mL reactor was added boron tribromide (1.0 M in CH_2Cl_2 , 0.5 mL, 0.5 mmol) and heated at 60°C for 2 min. Keeping the temperature, a chlorobenzene (0.5 mL) solution of 3,4,5,6-tetrafluorophthalonitrile (120 mg, 0.60 mmol, 2.4 eq.) was added dropwise into the reactor, and the reaction mixture was continually stirred for 2–4 hours until the starting material **3** was completely consumed. After removal of the solvent under vacuum, the residue was soon dealt with several drops of anhydrous THF (0.2 mL) and chromatographed on silica gel column (hexane: toluene = 2: 3) to remove impurities. The collected intermediate product was further treated with 4-fluorophenol (150 mg, excess amount) at 90°C for 2 h. Repeated chromatography (hexane: toluene = 2: 3) followed by recrystallization from CHCl_3 and hexane afforded the final enantiopure product **1** (26.0 mg, 0.032 mmol, 13%).

Computational details. M06 method with 6-311G(d) basis set was used in all calculations and carried out by *Gaussian 09 (Version D.01)* program³⁶. Wavefunction analyses including orbital composition analysis, electron transition density analysis, and transition dipole moment decomposition were processed by *Multiwfn (Version 3.3.8)* program³⁷. Calculation for the absorption frequencies of binaphthyl group (ν_{N}): The conformation of binaphthyl group under calculation is the same as that of **Bin** moiety in geometry-optimized molecule **1** and saturated by hydrogen (Fig. 2). Through TDDFT calculation, the first excited state was estimated to locate at 324 nm with large oscillator strength ($f = 0.21$). The conversion from absorption wavelength (λ) to frequency (ν) followed $\nu = c_0/\lambda$, where c_0 is the light speed. As a result, the corresponding absorption frequency ν_{N} for the first excited state was $0.93 \times 10^{15}\text{ s}^{-1}$. It is worth noting that the calculated ν_{N} was an estimated value that is qualitatively valid for calculating the factor $\nu_{\text{N}}\nu/(\nu_{\text{N}}^2 - \nu^2)$ (Table S2 in Supporting Information) and judging the chirality mechanism.

References

1. IUPAC. *Compendium of Chemical Terminology*, 2nd edn (Blackwell Scientific Publications, 1997).
2. Liu, M., Zhang, L. & Wang, T. Supramolecular chirality in self-assembled systems. *Chem. Rev.* **115**, 7304–7397 (2015).
3. Szumna, A. Inherently chiral concave molecules—from synthesis to applications. *Chem. Soc. Rev.* **39**, 4274–4285 (2010).
4. Kobayashi, N., Narita, F., Ishii, K. & Muranaka, A. Optically active oxo(phthalocyaninato)vanadium(IV) with geometric asymmetry: Synthesis and correlation between the circular dichroism sign and conformation. *Chem. Eur. J.* **15**, 10173–10181 (2009).
5. Mack, J., Stillman, M. J. & Kobayashi, N. Optically active phthalocyanines. *Coord. Chem. Rev.* **219–221**, 99–123 (2001).
6. Guerrero-Martínez, A. et al. Intense optical activity from three-dimensional chiral ordering of plasmonic nanoantennas. *Angew. Chem. Int. Ed.* **50**, 5499–5503 (2011).
7. Brückner, C. et al. Helimeric porphyrinoids: stereostructure and chiral resolution of meso-tetraaryl morpholinochlorins. *J. Am. Chem. Soc.* **133**, 8740–8752 (2011).
8. Maheut, G. et al. Chiroptical and computational studies of a bridled chirophthalocyanine and of its nickel(II), copper(II), and zinc(II) complexes. *J. Am. Chem. Soc.* **128**, 6347–6356 (2006).
9. Yang, L. et al. Stereochemistry and solid-state structure of an intrinsically chiral meso-patterned porphyrin: Case study by NMR and single-crystal X-ray diffraction analysis. *J. Org. Chem.* **78**, 9949–9955 (2013).
10. Zhao, L., Wang, K., Shang, H. & Jiang, J. Novel chiral ABBB-type unsymmetrical phthalocyanine. Ring-expansion synthesis, spectroscopic, and electrochemical properties. *Dyes Pig.* **120**, 52–56 (2015).
11. Wang, K. et al. Binuclear phthalocyanine-based sandwich-type rare earth complexes: Unprecedented two π -bridged biradical-metal integrated SMMs. *Chem. Eur. J.* **19**, 11162–11166 (2013).

12. Valev, V. K., Baumberg, J. J., Sibilica, C. & Verbiest, T. Chirality and chiroptical effects in plasmonic nanostructures: fundamentals, recent progress, and outlook. *Adv. Mater.* **25**, 2517–2534 (2013).
13. Claessens, C. G. & Torres, T. A new substitution pattern in subphthalocyanines: regioselective synthesis and separation of “ortho” derivatives. *Eur. J. Org. Chem.* 1603–1607 (2000).
14. Guillemé, J. *et al.* Non-centrosymmetric homochiral supramolecular polymers of tetrahedral subphthalocyanine molecules. *Angew. Chem. Int. Ed.* **54**, 2543–2547 (2015).
15. Zhao, L. *et al.* Synthesis and spectroscopic properties of chiral binaphthyl-linked subphthalocyanines. *Chem. Commun.* **50**, 7663–7665 (2014).
16. Shimizu, S. *et al.* Chiral 1,2-subnaphthalocyanines. *J. Am. Chem. Soc.* **133**, 17322–17328 (2011).
17. Kobayashi, N. & Nonomura, T. First observation of the circular dichroism spectra of chiral subphthalocyanines with C₃ symmetry. *Tetrahedron Lett.* **43**, 4253–4255 (2002).
18. Shang, H. *et al.* The first five-membered-heterocycle-fused subphthalocyanine analogues: chiral tri(benzo[*b*]thiopheno) subporphyrazines. *Chem. Eur. J.* **20**, 16266–16272 (2014).
19. Wakabayashi, M. *et al.* Anisotropic dissymmetry factor, *g*: theoretical investigation on single molecule chiroptical spectroscopy. *J. Phys. Chem. A* **118**, 5046–5057 (2014).
20. Shimizu, S., Nakano, S., Kojima, A. & Kobayashi, N. A core-expanded subphthalocyanine analogue with a significantly distorted conjugated surface and unprecedented properties. *Angew. Chem. Int. Ed.* **53**, 2408–2412 (2014).
21. Zhao, Y. & Truhlar, D. G. The M06 suite of density functionals for main group thermochemistry, thermochemical kinetics, noncovalent interactions, excited states, and transition elements: two new functionals and systematic testing of four M06-class functionals and 12 other functionals. *Theor. Chem. Acc.* **120**, 215–241 (2008).
22. Geuenich, D., Hess, K., Köhler, F. & Herges, R. Anisotropy of the induced current density (ACID), a general method to quantify and visualize electronic delocalization. *Chem. Rev.* **105**, 3758–3772 (2005).
23. Kobayashi, N., Ishizaki, T., Ishii, K. & Konami, H. Synthesis, spectroscopy, and molecular orbital calculations of subzaporphyrins, subphthalocyanines, subnaphthalocyanines, and compounds derived therefrom by ring expansion. *J. Am. Chem. Soc.* **121**, 9096–9110 (1999).
24. Kobayashi, N. *et al.* Substituent-induced circular dichroism in phthalocyanines. *J. Am. Chem. Soc.* **121**, 12018–12028 (1999).
25. Tinoco, I. Theoretical aspects of optical activity part two: polymers. *Adv. Chem. Phys.* **4**, 113–160 (1962).
26. Kobayashi, N. & Muranaka, A. *Circular dichroism and magnetic circular dichroism spectroscopy for organic chemists* (The Royal Society of Chemistry, 2012).
27. Zhou, Y. *et al.* Optical coupling between chiral biomolecules and semiconductor nanoparticles: size-dependent circular dichroism absorption. *Angew. Chem. Int. Ed.* **50**, 11456–11459 (2011).
28. Han, B. *et al.* Conformation modulated optical activity enhancement in chiral cysteine and Au nanorod assemblies. *J. Am. Chem. Soc.* **136**, 16104–16107 (2014).
29. Nakai, Y., Mori, T. & Inoue, Y. Theoretical and experimental studies on circular dichroism of carbo[n]helicenes. *J. Phys. Chem. A* **116**, 7372–7385 (2012).
30. Kumar, J., Nakashima, T. & Kawai, T. Circularly polarized luminescence in chiral molecules and supramolecular assemblies. *J. Phys. Chem. L* **6**, 3445–3452 (2015).
31. Cai, Y. *et al.* Enabling light work in helical self-assembly for dynamic amplification of chirality with photoreversibility. *J. Am. Chem. Soc.* **138**, 2219–2224 (2016).
32. Li, W. *et al.* Enantiospecific photoresponse of sterically hindered diarylethenes for chiroptical switches and photomemories. *Sci. Rep.* **5**, 9186 (2015).
33. Harada, N. & Nakanishi, K. *Circular dichroic spectroscopy exciton coupling in organic stereochemistry* (University Science Books, 1983).
34. Jurinovich, S. *et al.* The role of magnetic-electric coupling in exciton-coupled ECD spectra: the case of bis-phenanthrenes. *Chem. Commun.* **51**, 10498–10501 (2015).
35. Shimizu, S., Nakano, S., Hosoya, T. & Kobayashi, N. Pyrene-fused subphthalocyanine. *Chem. Commun.* **47**, 316–318 (2011).
36. Frisch, M. J. *et al.* (2013). *Gaussian 09, Version D.01*, Wallingford CT, United States. URL <http://www.gaussian.com/>.
37. Lu, T. & Chen, F. Multiwfn: A multifunctional wavefunction analyzer. *J. Comput. Chem.* **33**, 580–592 (2012).

Acknowledgements

We are grateful to Professor Benedetta Mennucci for kind help and a grant of EXAT tool package. Financial support from the National Key Basic Research Program of China (Grant Nos 2013CB933402 and 2012CB224801), Natural Science Foundation of China (No. 21290174), Beijing Municipal Commission of Education, and University of Science and Technology Beijing is gratefully acknowledged.

Author Contributions

L.Z. and J.J. designed the experiments and computation, and wrote the main paper. Z.T. also contributed to writing the main paper. D.Q., K.W. and T.W. helps the analyses of CD spectroscopy and calculation results. B.H. performed the CD and MCD measurements. All authors reviewed the manuscript.

Additional Information

Supplementary information accompanies this paper at <http://www.nature.com/srep>

Competing financial interests: The authors declare no competing financial interests.

How to cite this article: Zhao, L. *et al.* Integration of inherent and induced chirality into subphthalocyanine analogue. *Sci. Rep.* **6**, 28026; doi: 10.1038/srep28026 (2016).



This work is licensed under a Creative Commons Attribution 4.0 International License. The images or other third party material in this article are included in the article's Creative Commons license, unless indicated otherwise in the credit line; if the material is not included under the Creative Commons license, users will need to obtain permission from the license holder to reproduce the material. To view a copy of this license, visit <http://creativecommons.org/licenses/by/4.0/>